remote sensing

MDPI

Article

Assessing Satellite-Derived Shoreline Detection on a Mesotidal Dissipative Beach

Carlos Cabezas-Rabadán [1,2,*], Jaime Almonacid-Caballer [1], Javier Benavente [3], Bruno Castelle [2], Laura Del Río [3], Juan Montes [3,4], Jesús Palomar-Vázquez [1] and Josep E. Pardo-Pascual [1]

[1] Geo-Environmental Cartography and Remote Sensing Group (CGAT-UPV), Department of Cartographic Engineering, Geodesy and Photogrammetry, Universitat Politècnica de València, Camí de Vera s/n, 46022 Valencia, Spain; jaialca@upvnet.upv.es (J.A.-C.); jpalomav@upvnet.upv.es (J.P.-V.); jepardo@cgf.upv.es (J.E.P.-P.)
[2] Univ. Bordeaux, CNRS, Bordeaux INP, EPOC, UMR 5805, F-33600 Pessac, France; bruno.castelle@u-bordeaux.fr
[3] Department of Earth Sciences, INMAR (Marine Research Institute), University of Cádiz, 11003 Puerto Real, Spain; javier.benavente@uca.es (J.B.); laura.delrio@uca.es (L.D.R.); juan.montes@uca.es (J.M.)
[4] Department of Physics and Earth Sciences, University of Ferrara, 44121 Ferrara, Italy
* Correspondence: carcara4@upv.es

Abstract: The accuracy and robustness of the shoreline definition from satellite imagery on different coastal types are crucial to adequately characterising beach morphology and dynamics. However, the generic and widespread application of satellite-derived shoreline algorithms is limited by the lack of robust methods and parameter assessments. This work constitutes a quantitative and comprehensive assessment of the satellite-derived waterlines from Sentinel-2 by using the novel SAET tool (Shoreline Analysis and Extraction Tool) on the exposed and mesotidal beach of La Victoria (Cádiz, SW Spain). The diverse parameters available in SAET, such as water indexes, thresholding methods, morphological filters, and kernel sizes, were combined to define water/land interface positions that were compared against coincident video-derived waterlines. Satellite-derived waterline errors are found to be affected by extraction parameters, as well as by the oceanographic and morphological conditions at the time of the image acquisition. The application of a morphological erosion filter on the water mask, which tends to shift the extracted waterline seawards and reduce bias, is the best solution at the dissipative site of La Victoria Beach. Moreover, using a 3 × 3 kernel size consistently shows higher accuracies than a larger kernel. Although there was no parameter combination showing the best skill for all dates, the employment of the Automated Water Extraction Index for images with no shadows (AWEInsh) with a threshold = 0, erosion morphological filter, and 3 × 3 kernel was, overall, the best combination of extraction parameters for this beach (average waterline RMSE of 5.96 m). The combination of the Modified Normalised Difference Water Index (MDNWI) with the Otsu thresholding also led to similar positions of the resulting waterlines and offered good accuracies. In line with other recent research efforts, our work stresses the lack of generic shoreline extraction solutions that can be applied automatically at a global level and the necessity to adapt and validate the extraction methodologies to the different types of coastlines.

Keywords: shoreline definition; Sentinel-2; beach monitoring; water indexes; videomonitoring; SAET

Citation: Cabezas-Rabadán, C.; Almonacid-Caballer, J.; Benavente, J.; Castelle, B.; Del Río, L.; Montes, J.; Palomar-Vázquez, J.; Pardo-Pascual, J.E. Assessing Satellite-Derived Shoreline Detection on a Mesotidal Dissipative Beach. *Remote Sens.* **2024**, *16*, 617. https://doi.org/10.3390/rs16040617

Academic Editors: José Juan de Sanjosé Blasco, Germán Flor-Blanco and Ramón Blanco Chao

Received: 11 January 2024
Revised: 2 February 2024
Accepted: 4 February 2024
Published: 7 February 2024

1. Introduction

An efficient management of the coast requires accurate, updated, and homogeneous data about the beach morphology. The shoreline position provides quantitative information about the morphological state of the beaches and its changes [1], thus serving as, e.g., a valuable indicator for understanding long-term shoreline trend and their driver(s) [2], linking shoreline variability with climate modes of atmospheric and/or oceanographic

variability [3], and forecasting future scenarios [4]. These applications are essential for supporting decision-making processes in the face of the diverse erosion problems that affect the coasts worldwide (e.g., [5–8]), therefore constituting one of the main issues in coastal zone management. Earth observation data have the potential to offer valuable information for the characterisation of coastal morphological changes from a local to a global scale and with high temporal resolution [9]. An example of this is the optical imagery captured by the Sentinel-2A and 2B satellites provided by the European Commission through the European Space Agency (ESA). The challenge lies in accurately defining the water boundary, considering the limitations imposed by the pixel size of the satellite images. Satellite-derived shoreline (SDS) algorithms such as CoastSat [10], SHOREX [11], and CASSIE [12] have tackled this challenge by devising efficient approaches to overcome such limitations (see review and benchmark comparison in Vos et al. [13]). Sustained in the subpixel solution proposed by Pardo-Pascual et al. [14] and in the workflow followed by SHOREX, the tool SAET [15] has appeared as a new alternative focused on offering high autonomy, efficiency and robustness in the extraction. This goal is accomplished by enabling its application along large coastal segments while tuning the settings and extraction parameters according to the respective coastal characteristics.

The strategies followed, and the extraction parameters employed for defining the shoreline influence its final positioning. Many of the current extraction approaches, particularly those based on the analysis of the maximum gradient [9], proceed to locate the approximate pixel shoreline (APS) so that, subsequently, a refining process leads to the final position with sub-pixel accuracy. The location of the APS can be sustained not only by analysing the original bands but also by combinations of them known as indices. Among these, the prominent ones include those oriented towards highlighting the radiometric differences between the water and the land, therefore enabling the thresholding of the water bodies. This is the case of the MNDW index developed by Xu [16] and employed by CoastSat [10] and the AWEI index proposed by Feyisa et al. [17]. In turn, AWEInsh with a 0 threshold has appeared as a robust and accurate method for shoreline extraction both at oceanic coasts [18] and inland water bodies [19].

Regarding the techniques to binarise a given index, the use of a single threshold value to distinguish the water and the land (theoretically being 0) is a straightforward and efficient approach (e.g., [19,20]). Alternatively, binarisation can be accomplished using methods such as Otsu thresholding [21]. This method performs a separation of the classes (zones) present in the coastal strip by calculating the histogram of the image and defining zones with a minimised inner variance (e.g., [10,22]). Both thresholding methods were included in the workflow followed by SAET as they are commonly employed by the different extraction tools and algorithms [23]. Nevertheless, there are no robust comparisons to support the advantages of one or the other, and the combination of indices and thresholds for an optimal extraction in different coastal types is still unknown [9].

After the binarisation, the approximate shoreline can be identified from the water mask by applying different mathematical morphological filters [24], such as dilation and erosion. Considering the instantaneous interface between the water (sea) and the land (emerged beach) or waterline (WL), the APS can be defined either as the first line of land pixels in contact with water (erosion filter) or as the first line of water pixels in contact with land (dilation). Thus, taking the 'water' class as a reference, the dilation would define the APS in the first line of pixels landward, while the erosion would define the APS in the first line of pixels seaward. The effects of using these morphological filters on the positioning of the resulting WL have been preliminarily evaluated for the case of SAET [18]. The results indicate that when using the maximum gradient method (and for the same kernel size), the employment of a dilation or erosion filter can significantly influence the precision (bias) of the resulting WL in specific coastal typologies.

Once the approximate line is defined, the sub-pixel refinement process leads to the definition of the satellite-derived waterlines (SDWLs). To achieve this, the maximum gradient points are identified by analysing the digital levels within a neighbourhood of

analysis (kernel) and fitting a polynomial function to the digital levels of the pixels in that area (see [14]). As long as the APS is accurately determined, a smaller kernel size could potentially result in a more precise positioning of the SDWL. However, although this assumption has proven correct for extraction tools such as SHOREX [11], it has not been verified within the context of SAET.

The position of the WL depends on the elevation of the water level, which is defined by the instantaneous waves and tide conditions in combination with the beach morphology. Thus, WL position shifts cross-shore over time by a magnitude proportional to the elevation of the water level and inversely proportional to the slope of the beach. From the instantaneous information provided by the WLs, the shoreline positions can be obtained by referencing the WL positions to a single reference elevation datum [25,26]. This can be accomplished by horizontally shifting the SDWLs according to their instantaneous total water level and the local slope. The resulting positions referenced to the same datum constitute the SDSs, which enable the robust analysis of changes over time. The magnitude of the SDWL errors may be influenced by different factors. While some of the errors are inherent to the image characteristics, such as their geo-referencing (which can be minimised using cross-correlation techniques, see [27]), the definition of the SDWL position greatly depends on the extraction tools and the diverse parameters defining the extraction processes. The presence of foam can lead to gross errors in the detection [22,26], probably by affecting the APS definition. At the same time, different authors have pointed out how the run-up and swash phenomena lead to uncertainties in the realities represented by the SDWLs (e.g., [28,29]). The extraction tools seem to offer higher accuracies when the transition between the water and the land is clearly defined, while the errors increase associated with more diffuse interphases. This mainly appears associated with gentle slopes [13,18,30] and tidal environments, especially during low tide conditions when saturated areas and complex intertidal morphologies appear [29]. At this point, the potential to adapt the extraction methods according to diverse coastal conditions needs to be explored to achieve the highest possible accuracy when defining the SDWL and, subsequently, the SDS.

SAET is a versatile tool that enables choosing among different parameters and methods for defining the approximate and the subpixel WL [15]. Their combined testing was preliminarily addressed by Pardo-Pascual et al. [18] across a variety of coastal types. However, this assessment was limited to a single date per site and only included a reduced number of dissipative beaches. This study aims to evaluate SAET performance on a mesotidal dissipative beach with complex intertidal morphologies, regarding (a) how the extraction parameters and segmentation methods condition the accuracy when defining the instantaneous WL, (b) the influence of the morphological and oceanographic conditions on the resulting errors, enabling (c) to discuss the most favourable combinations of extraction parameters for this type of beach and to present some recommendations for the shoreline extraction. Video-derived waterlines (VDWLs) from a mesotidal dissipative beach were used as ground truth to assess a series of instantaneous SDWLs defined over one year using SAET.

2. Methods

The analysis consists of the assessment of 19 SDWLs obtained on La Victoria beach (Cádiz) from Sentinel-2 (S2) images using SAET by comparing their position against simultaneous VDWLs.

2.1. Study Site

The study site is located in the urban beach of La Victoria (Cádiz, SW Spain). The beach extends about 3 km following NNW-SSE orientation in the outer part of the Bay of Cádiz (Figure 1). It is located at a sandy barrier system that separates the inner area of the Bay of Cádiz from the Atlantic Ocean. The landward limit of the beach is defined by a promenade built upon the ancient dune system, while its northern limit is constituted by groins and an intertidal rocky shore platform. Regarding the submerged part of the

beach, a rocky shore platform formed by a bioclastic conglomerate and quarzitic rocks extends alongshore discontinuously, with varying widths and depths being its highest part emerged in spring low tides [31,32]. La Victoria beach is composed of fine sands (grain size 0.22 mm; [33]) and shows an intermediate-dissipative slope, with the common presence of complex morphologies in the intertidal zone, such as wide and flat swash bars and cusp systems [34].

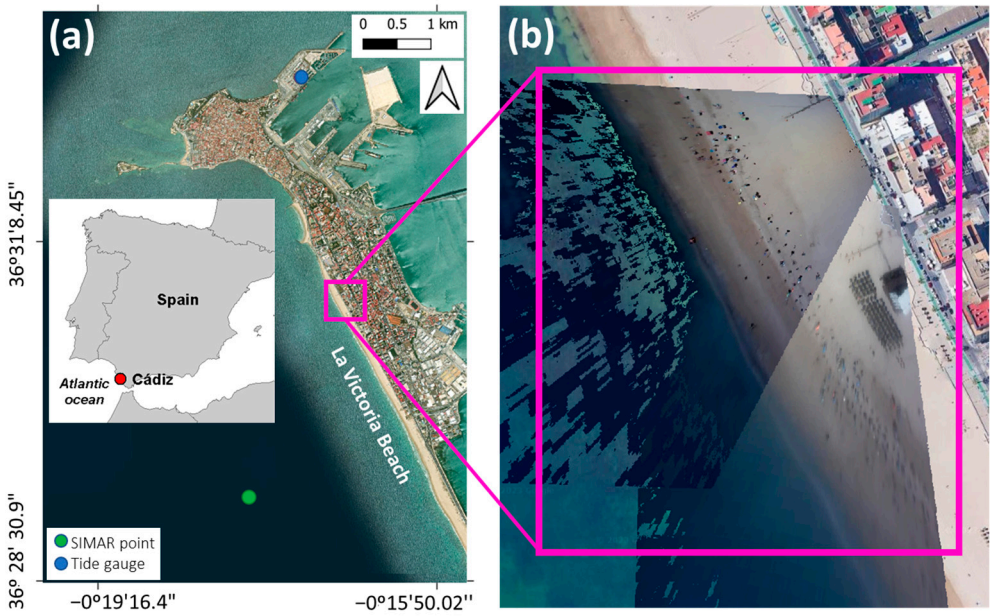

Figure 1. (**a**) Location map of the study area in La Victoria Beach in Cádiz (SW Spain) including the SIMAR point (green) and the tide gauge (blue) employed for retrieving wave and sea level data. (**b**) Mosaic of the projected images on 26 July 2018 from the video-monitoring system. Background orthophotograph PNOA 2019 CC BY 4.0 www.scne.es (accessed on 9 January 2023).

Regarding the hydrodynamic regime, tides are semi-diurnal and mesotidal, with a Mean Spring Tidal Range (MSTR) of 3.06 m. Average wave height is below 1 m with associated periods of 5–6 s. However, wave height during westerly storms, which occur mainly between November and March, can exceed 4 m [33]. The dominant longshore drift is directed towards the southeast.

2.2. Oceanographic and Morphological Conditions

Specific oceanographic and morphological data coincident with the study period (2018) were retrieved in order to enable an in-depth analysis of their relationship with the WL behaviour (Figure 2a). According to the satellite images free of clouds employed in the assessment, the wave data (Hs and Tp) and sea level data (SL) were retrieved at the time of the satellite passage (systematically acquired at 11:15 GMT, Table 1). Furthermore, to allow the characterisation of the tidal state at the time of the image acquisition, the SL was also retrieved one hour before and one hour after. Subsequently, it was possible to characterise the tidal state for the instant of the image acquisition. Regarding the beach morphology, 9 topographic surveys were carried out during 2018 (Figure 2b) using an RTK-DGPS, allowing the definition of the intertidal beach slope (see [35]).

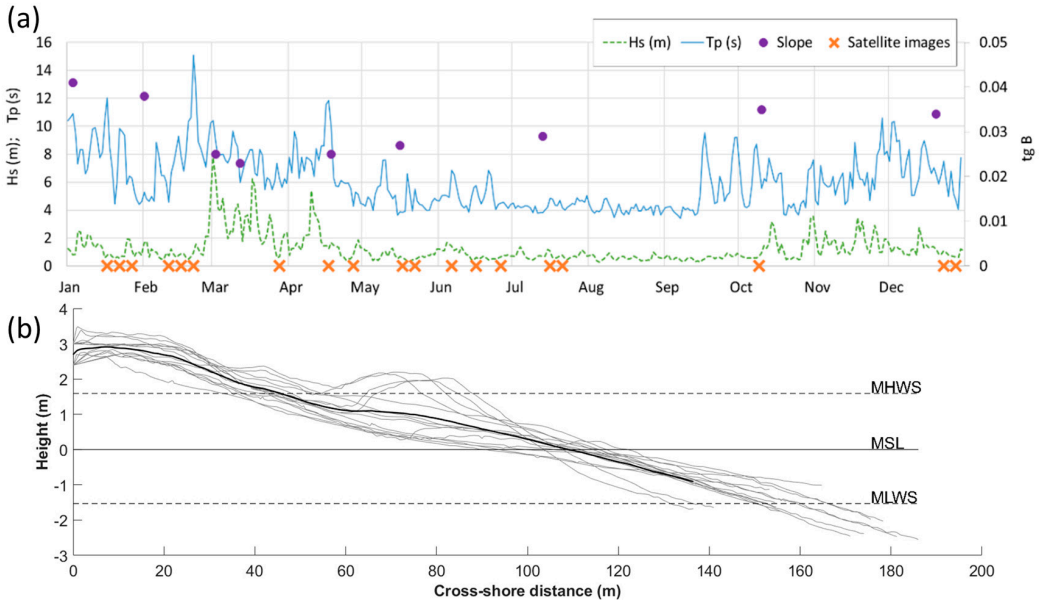

Figure 2. (**a**) Wave data (daily maximum Hs and Tp, presented as dashed green and solid blue lines) from the modelled point SIMAR 6012044 (see location in Figure 1) from Puertos del Estado (https://www.puertos.es/, accessed on 9 January 2023) together with the beach-face slope estimated from topographic surveys (purple dots) and the availability of S2 satellite images (orange crosses). (**b**) Topographic profiles from 2018 field surveys (average profile highlighted as a thick black line), and values for the Mean High Water Spring (MHWS) and Mean Low Water Spring (MLWS).

Table 1. Oceanographic conditions at the time of the S2 image acquisition. Sea level data were obtained one hour before and after the acquisition of the satellite images from the tide gauge located at Port of Cádiz by the Spanish Institute of Oceanography (http://indamar.ieo.es/mareas/mareas.htm, accessed on 9 January 2023, see location in Figure 1) taking MSL as reference. Significant wave height (Hs), average period (Tm) and peak period (Tp) were obtained from the SIMAR point 6012044 (see Figure 2).

Date (DD-MM-YY)	SL (m) acquisit. Time −1 h	SL (m) 11:15 GMT	SL (m) acquisit. Time +1 h	Tidal State	Hs (m)	Mean Period (s)	Tp (s)
17-01-18	−0.847	−0.357	0.183	rising	0.56	7.82	14.01
22-01-18	−0.967	−1.087	−0.997	low	0.31	4.18	3.81
27-01-18	0.863	0.783	0.523	falling	0.53	5.78	4.64
11-02-18	0.403	0.603	0.603	high	0.41	6.05	4.03
16-02-18	−0.947	−0.437	0.163	rising	0.71	9.17	14.48
21-02-18	−1.087	−0.977	−0.917	low	0.6	9.89	11.23
28-03-18	0.563	0.993	1.173	rising	0.43	7.19	9.32
17-04-18	−1.247	−0.797	−0.187	rising	0.68	7.82	10.02
27-04-18	0.323	0.943	1.333	rising	0.35	5.23	4.23
17-05-18	−1.177	−0.737	−0.107	rising	0.25	3.71	3.49
22-05-18	0.643	0.283	−0.107	falling	0.34	3.83	3.76
06-06-18	0.193	−0.077	−0.327	falling	0.69	4.92	8.33
16-06-18	−1.247	−0.977	−0.557	rising	0.5	5.03	4.45
26-06-18	0.003	0.503	0.953	rising	0.45	4.2	4.24
16-07-18	−1.237	−1.207	−0.867	low	0.48	3.88	4.21
21-07-18	0.803	0.603	0.283	falling	0.48	3.82	4.21
09-10-18	−0.507	0.143	0.903	rising	0.51	8.98	11.16
23-12-18	−0.957	−0.357	0.393	rising	0.97	5.79	12.11
28-12-18	−0.257	−0.777	−0.987	falling	0.5	5.11	7.52

2.3. Video-Derived Waterlines

In order to assess the spatial accuracy of the SDWLs, the VDWLs constituted the ground-truth data for this analysis. The video monitoring system located at La Victoria Beach (see [34] for further details) consists of 3 IP cameras (1600 × 1200 pixels resolution) installed 49 m above mean sea level. The cameras cover about 750 m alongshore, including the surf and the intertidal zones, the dry beach, the promenade, and the adjacent street. The system records 10 min of video per hour (MPEG-4 format, 4 Hz), and it allows the automatic extraction of the Snap (snapshot) and Timex (time-exposure) images using the system ORASIS [36].

The images acquired by the video monitoring system were projected at sea level at the time of acquisition of the satellite image, leading to the obtention of the ground-truth data following the procedures suggested by Sánchez-García et al. [37] and Simarro et al. [38]. The processing of the images followed three steps (Figure 3): (a) calibration, (b) co-registration, and (c) geo-projection. The calibration consisted of calculating the internal parameters of the cameras (i.e., distortions of the lenses), which enabled the undistorting of the images. The co-registration comprised the overlapping of the images to remove potential little displacements over time, therefore enabling the use of ground control points (GCPs) on every image. The geo-referenced projection involved the orientation of the images according to the GCPs, and subsequently, each image was projected over the horizontal plane according to the instantaneous sea level. During this third step, each pixel experienced a deformation as its footprint was projected. Although projected images presented a spatial resolution of 0.25 m/pixel, the farther a pixel was projected, the larger its footprint was, leading to footprint differences between the original and the projected pixels. The farthest projected pixel of the central camera presented a footprint of 6 projected pixels, i.e., 1.5 m in line from the camera position, which could translate into a lower accuracy during the photo interpretation. In order to allow a robust definition of the VDWLs, the farthest camera was removed from the study. Thus, only the closest two cameras were employed for the assessment, leading to an analysed coastal segment of about 375 m (see Figure 1b).

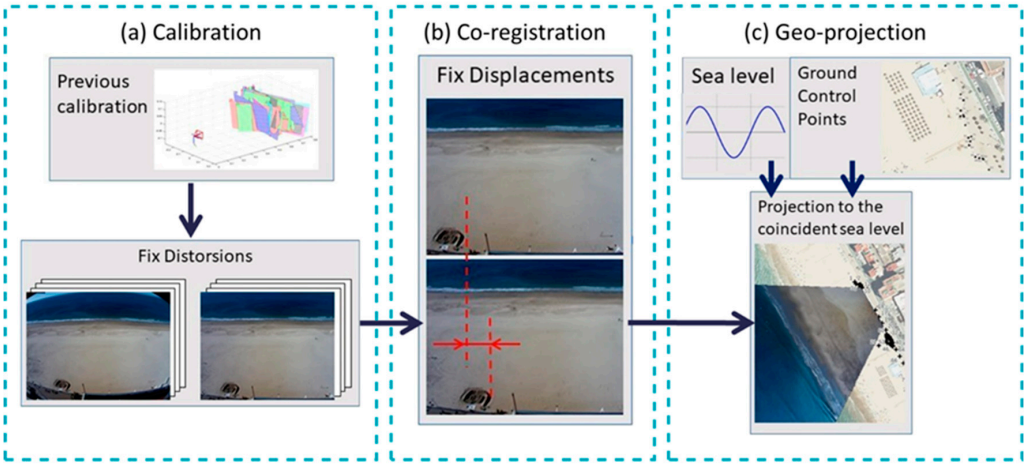

Figure 3. Workflow for the definition of the VDWLs.

The WL was manually digitised on the projected images by two expert users using both Timex and Snap images. The photo-interpreters (P1 and P2) found that the WL appeared more clearly defined on the Timex images (derived from the information acquired for 10 min), leading to smaller uncertainties and, therefore, allowing a more robust photo-interpretation. To validate the use of the reference lines derived from the Timex images, their positions were compared to quantify the magnitude of the uncertainty caused by the photo-interpretation process. On average, small differences appeared when comparing both photo-interpreters and types of images (Table 2, Figure 4). Thus, the higher certitude

in the photo-interpretation, together with the small differences that emerged between users and methods, led to the selection of the reference lines identified from Timex (P1) for subsequent evaluations. Nevertheless, when analysing the dates individually (Figure 4), the VDWLs on 21 February were discarded from the assessment as important differences appeared between the positions defined by both photo-interpreters, with a magnitude remarkably higher than for the rest of the dates.

Table 2. Differences in the spatial location of the VDWLs (expressed as RMSE, in m) defined from both types of images (Timex and Snap) by two photo-interpreters (P1 and P2). The average differences were calculated considering Timex_P1 as the reference, with the positive (negative) values representing a seaward (landward) bias.

Error (m)	Snap_P1	Snap_P2	Timex_P2
Mean ± SD	−0.49 ± 1.14	0.73 ± 1.69	1.01 ± 1.58
RMSE	1.51	2.31	2.23

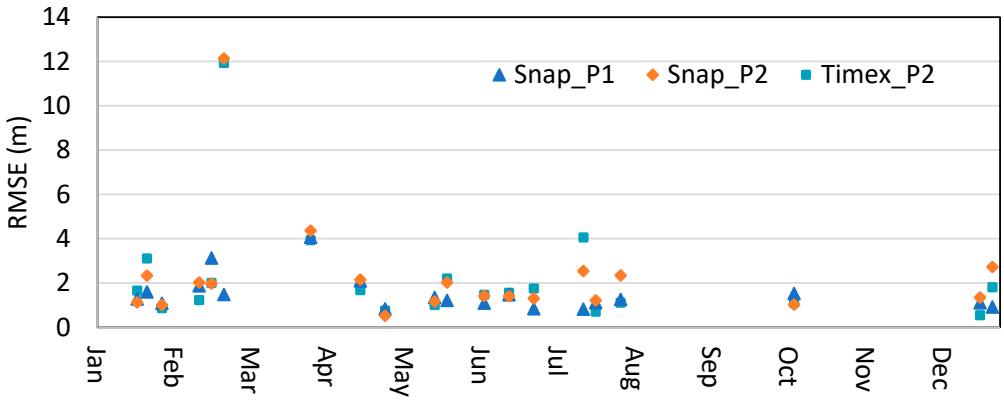

Figure 4. Differences in the spatial location of the VDWLs expressed as RMSE (in m) defined by the two photo-interpreters (P1 and P2) from both types of images (Timex and Snap). The differences were calculated for the studied dates considering the first photo-interpreter (P1) and the Timex images as the reference.

2.4. Detection of the Waterline from Satellite Imagery

The instantaneous SDWLs were defined from the freely available optical Sentinel-2 imagery using the software SAET v4 (https://github.com/jpalomav/SAET_master) with different configuration parameters (Figure 5). The workflow followed four main phases (see details in [15]) comprising the image downloading, the segmentation for defining the APS, its masking, and the final extraction of the sub-pixel waterline.

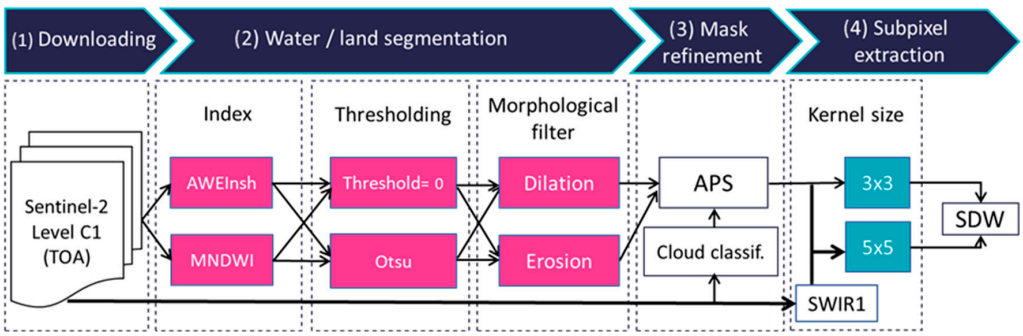

Figure 5. Workflow with the combination of extraction parameters included in the assessment. water indexes, thresholding methods, and morphological filters that have been tested appear highlighted (pink colour) as well as the kernel sizes (emerald).

1. Image downloading. The S2 images with a cloud coverage below 30% were downloaded via the Copernicus Open Access Hub (https://scihub.copernicus.eu/, accessed on 1 August 2023). Top-Of Atmosphere (TOA) images were employed as the atmospherically corrected images (Bottom-of-Atmosphere, BOA) did not provide significant improvements in the SDWL accuracy in previous tests [18].
2. Water/land interface segmentation. The WL was characterised by the limit of the water mask. This mask was defined employing different water indexes, thresholding methods, and morphological filters to assess their effect on the positioning of the resulting APS and, subsequently, the subpixel waterline (see pink squares in Figure 5). For each image, the two water indices were computed, AWEInsh (Equation (1), as originally described by Feyisa et al. [17] and the MNDWI (Equation (2), described by Xu [16]), being subsequently binarised using both a constant threshold = 0 and the thresholding method by Otsu [21], and finally defined the continuous sets of pixels that constitute the limit of the water mask (i.e., the water/land interface) by applying the morphological filters of dilation and erosion (that would displace it landward/seawards, respectively).

$$\text{AWEInsh} = 4 \cdot (\text{G} - \text{SWIR1}) - (0.25 \cdot \text{NIR} + 2.75 \cdot \text{SWIR2}) \quad (1)$$

$$\text{MNDWI} = (\text{G} - \text{SWIR1})/(\text{G} + \text{SWIR1}) \quad (2)$$

   with NIR, SWIR1, SWIR2 and G the values of the pixel intensity in the near-wave infrared, short-wave infrared 1, short-wave infrared 2, and green bands, respectively.
3. Water–land mask refinement. Considering the water/land interface of the water mask as input, the APS was defined after removing pixels classified as clouds according to the cloud classification bands provided by the image servers.
4. Sub-pixel extraction. Following the pixels defined by the APS, the waterline was identified at the subpixel level. For this purpose, a kernel analysis of two different sizes (3×3 and 5×5 pixels; see emerald squares in Figure 5) was performed on the SWIR1 band. The sub-pixel location was defined by the points (every 5 m) where the reflectance values show the highest gradient edge. This step was accomplished by employing the algorithm described in Pardo-Pascual et al. [14]. To finish the process, the minimum spanning tree method [39] was applied to remove outliers and obtain the final SDWL as proposed by Sánchez-García et al. [11].

2.5. Accuracy Assessment

The accuracy of the waterlines resulting from the combination of different extraction parameters was compared with the reference lines derived from ground-truth data, i.e., VDWLs. The accuracy (error) of each SDWL was defined by planimetrically comparing the position of its vertices (points every 5 m alongshore) against its respective reference line (Timex_P1). This step was carried out by measuring the shortest distance between each of the points composing the SDWL and the photo-interpreted VDWLs. The accuracy results from the combination of different extraction parameters were presented with the statistics of the errors: bias (mean distance), precision (standard deviation, hereafter SD), and accuracy (root mean square error, RMSE). According to those values, the most efficient combinations of image processing levels were identified, and the impact of the oceanographic characteristics of each date on the resulting errors was analysed.

For the different combinations of extraction parameters proposed, the relationship between the SDWL accuracy on the different dates and the parameters describing the oceanographic and morphological conditions (see Figure 2) was analysed. Thus, the positioning errors of the SDWLs were compared with the sea level and the relative state of the tide (falling, low, and rising), the parameters characterising the waves such as Hs, Tp, total water level, run-up (according to Stockdon et al. [40]) and wave factor (understood as the product of Hs and Tp), and the slope of the beach.

3. Results

For each date, the waterline position was extracted using two water indexes (for water/non-water pixel classification), two thresholding methods (to binarise the water indexes and obtain a water mask), two morphological operations (to obtain the APS) and two kernel sizes (to obtain the sub-pixel SDWL). This led to a total of 16 combinations (hereafter C1 to C16) or evaluation cases. The errors registered on the 18 analysed dates were summarised enabling the identification of the combinations of parameters that lead to the highest accuracies (Table 3). Note that a positive (negative) bias indicates that the SDWL is located seaward (landward) of the VDWLs.

Table 3. Average error expressed by the bias (mean distances), precision (standard deviation, SD) and accuracy (RMSE) of the SDWL series obtained using different kernel sizes, mathematical morphological filters, indexes, and thresholding methods. Seaward (landward) displacements are represented by positive (negative) values. For each descriptor of the error, the lowest values are highlighted in bold.

Combination	Extraction Parameters	Bias (m)	SD (m)	RMSE (m)
1	3 × 3, Erosion, AWEInsh, 0	2.70	**2.28**	**5.96**
2	3 × 3, Erosion, AWEInsh, Otsu	−4.39	2.51	7.64
3	3 × 3, Erosion, MNDWI, 0	−3.15	2.40	6.65
4	3 × 3, Erosion, MNDWI, Otsu	**0.82**	2.42	7.22
5	3 × 3, Dilation, AWEInsh, 0	−8.76	2.22	9.34
6	3 × 3, Dilation, AWEInsh, Otsu	−17.16	2.87	17.48
7	3 × 3, Dilation, MNDWI, 0	−15.44	2.67	15.74
8	3 × 3, Dilation, MNDWI, Otsu	−10.92	2.57	11.95
9	5 × 5, Erosion, AWEInsh, 0	−10.30	5.34	12.39
10	5 × 5, Erosion, AWEInsh, Otsu	−14.09	2.77	14.60
11	5 × 5, Erosion, MNDWI, 0	−13.64	2.95	14.26
12	5 × 5, Erosion, MNDWI, Otsu	−13.59	3.43	14.57
13	5 × 5, Dilation, AWEInsh, 0	−14.58	2.51	14.92
14	5 × 5, Dilation, AWEInsh, Otsu	−17.67	2.79	18.00
15	5 × 5, Dilation, MNDWI, 0	−17.20	2.71	17.53
16	5 × 5, Dilation, MNDWI, Otsu	−15.10	2.58	15.52

Clear differences appeared in the magnitude of the errors according to the neighbourhood of analysis (Table 4). Thus, the 3 × 3 kernel size (combinations 1–8) consistently performed better than 5 × 5 (combinations 9–16), mainly due to the substantially lower bias (7 m and 14.5 m seawards, respectively). On the other hand, the thresholding method did not seem to offer consistent differences in the results. The influence of the thresholding on the errors seemed to appear when combined with the other extraction parameters, particularly with the morphological filter.

Table 4. Average errors of the waterlines extracted when employing different indices, thresholding methods, mathematical morphological filters, and kernel sizes.

	Index		Thresholding		Morph. Operation		Kernel Size	
Error (m)	**AWEInsh**	**MNDWI**	**0**	**Otsu**	**Erosion**	**Dilation**	**3 × 3**	**5 × 5**
SD	2.91	2.72	2.89	2.74	3.01	2.62	2.49	3.14
RMSE	10.91	13.99	13.06	12.10	10.49	14.35	10.00	14.78

The combinations, including the morphological filter of erosion (combinations 1–4 and 9–12), performed better than those employing the dilation (5–8 and 13–16). In most cases, dilation led to errors above 10 m RMSE, mainly due to large differences regarding the bias (about 7 m and 14 m seawards, respectively). Among those employing the dilation, the only exception appeared when using the index AWEINSH and the thresholding = 0 (combination five). This was the combination that offered the lowest bias (8.76 m landwards)

and the lowest standard deviation (2.22 m), leading to the highest accuracy (9.34 m RMSE). The best accuracies appeared when employing the kernel 3 × 3 together with the erosion filter (Figure 6). This way, combination one, which employed the AWEInsh index with a threshold = 0, the erosion filter, and a 3 × 3 kernel, reached the best results overall. This combination provided the lowest errors, both regarding the precision (2.28 m) and accuracy (5.96 m RMSE) and the second lowest bias (2.70 m), while the lowest one (0.82 m) appeared with combination four. Nevertheless, the higher standard deviation (2.42 m) translated into a lower accuracy (7.22 m RMSE). Both combinations, one and four, were the only ones that led to seaward-displaced waterlines. On the contrary, combinations two and three led to waterlines being displaced landward, which resulted in lower accuracy even when showing similar levels of precision (2.51 and 2.40 m of standard deviation).

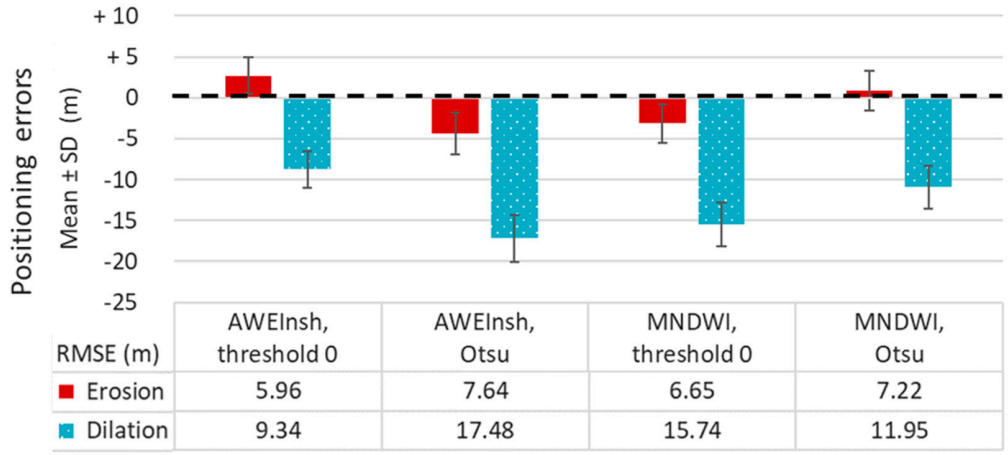

RMSE (m)	AWEInsh, threshold 0	AWEInsh, Otsu	MNDWI, threshold 0	MNDWI, Otsu
Erosion	5.96	7.64	6.65	7.22
Dilation	9.34	17.48	15.74	11.95

Figure 6. Errors of the SDWLs, expressed by the mean distance (bias), standard deviation and RMSE, obtained when using a 3 × 3 kernel size and different index, thresholding method and mathematical morphological filter (combinations of parameters 1–8).

When plotting the errors obtained throughout the year (Figure 7) by using combinations one to four, there is no evidence of a clear seasonal pattern. It can be seen how, on certain dates, accuracy errors (RMSE) are mainly caused by higher bias, while on other occasions, they are related to a low precision (high SD). Also, when analysing the distribution of errors versus the pattern of incident waves and slope changes (see Figure 2) along the year, no clear relationship between the different factors is observed. Although the swell episodes at the beginning of the year and early spring seem to be linked to a decrease in beach slope, these two factors do not show any clear relationship with the errors recorded by the SDWLs. Thus, some of the SDWLs with the highest errors appear on dates with low waves and with a beach profile that is not excessively steep (e.g., 22 May and 28 December when employing combination one).

Regarding the magnitude of the errors achieved by the different combinations of parameters, a similar pattern appeared over time, although important differences arose in certain dates. The relationship between the tidal level and the waterline errors was analysed, showing that certain combinations of parameters were more prone to lead to positioning differences in the SDWLs according to reductions in the tidal level (Figures 7 and 8, Table 5). Thus, C2 and C3 presented moderate correlations (expressed as R^2) between the tidal level and the bias (0.396 and 0.217) and the RMSE (0.549 and 0.341). On the contrary, the correlation was almost negligible when employing C1 and C4 (R2 < 0.2 for all the parameters describing the error).

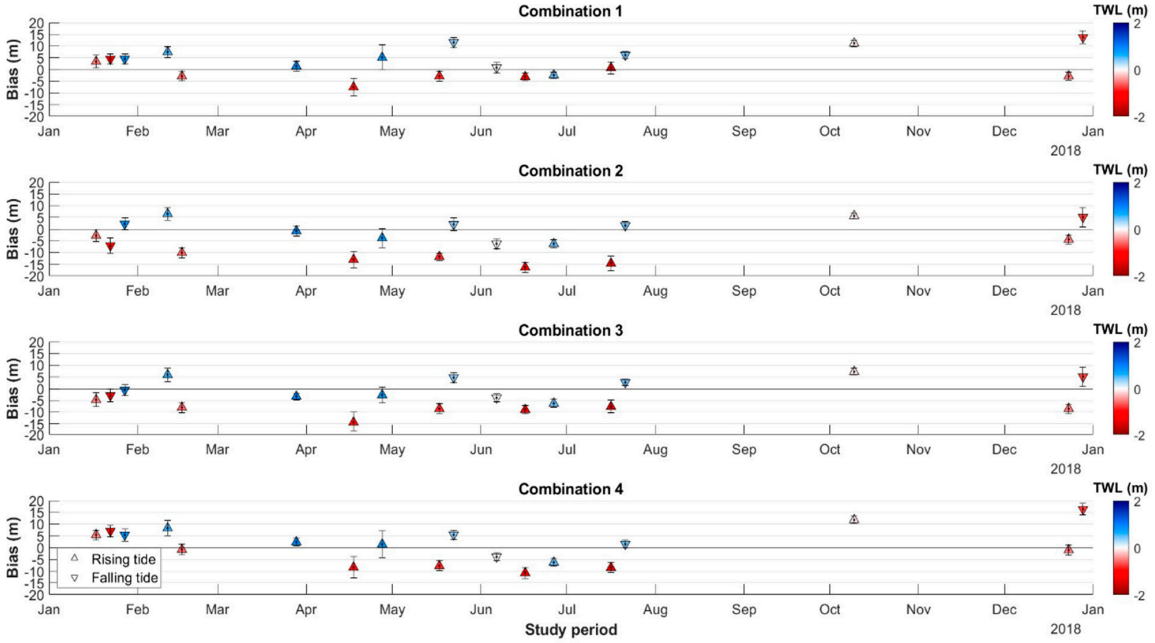

Figure 7. Errors (as bias ± SD, in m) of the resulting waterlines for combinations 1–4 of extraction parameters. The total water level (TWL) is presented in different colours, while the different symbols describe the rising (triangle pointing upwards) and falling tide (downwards) conditions.

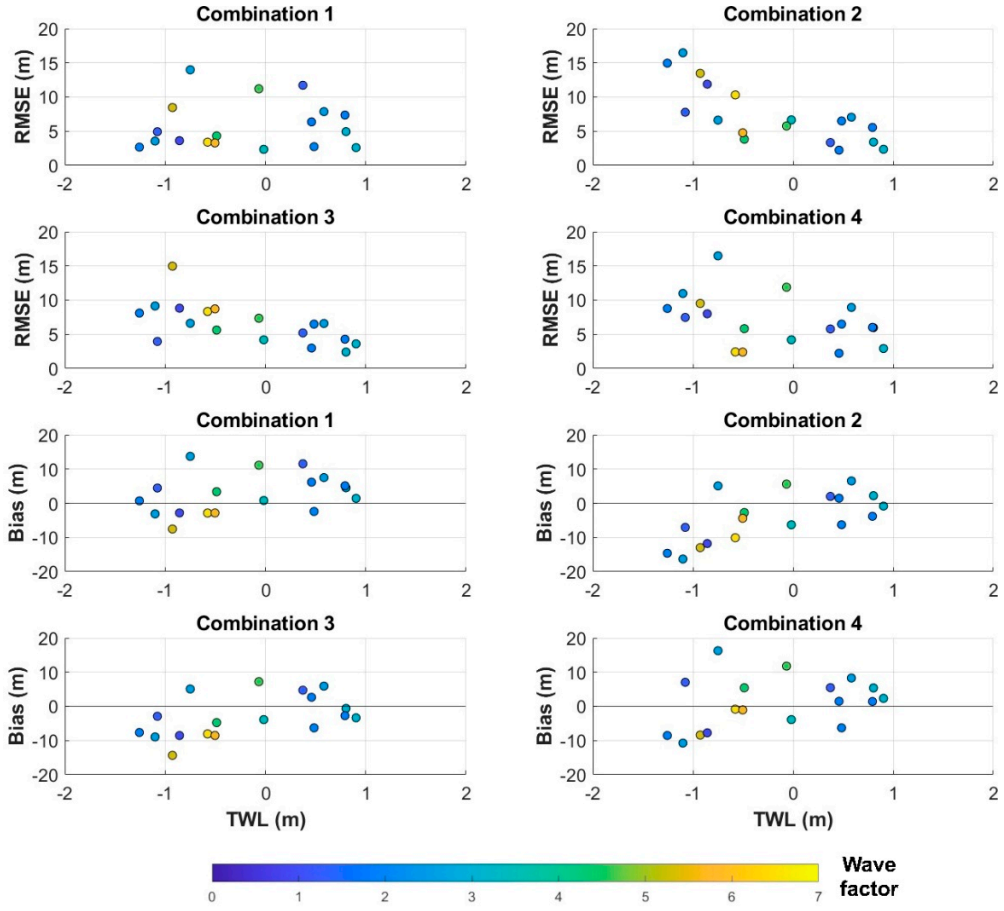

Figure 8. Relationship between tide level and the waterline errors, defined by the bias and the RMSE for the combinations 1–4 of extraction parameters. The wave factor (as the product of Hs and Tp) is presented by the different colours of the points.

Table 5. Relationship, defined by linear correlations (expressed as R^2) between tide level and the waterline errors (defined by the bias, the SD and the RMSE), for the combinations 1–4 of extraction parameters. The combination showing the highest value for each type of error is highlighted.

Combination	Bias	SD	RMSE
1	0.097	0.002	0.005
2	**0.396**	0.039	**0.549**
3	0.217	**0.136**	0.341
4	0.085	0.010	0.178

To analyse the effect of the tidal conditions on the overall accuracy, different SDWLs were discarded from the analysis according to the tide level. Thus, it is observed that when discarding the two SDWLs associated with low tide conditions, overall errors slightly improved for the different combinations of parameters. Thus, the standard deviation was reduced by 7% overall, and the RMSE was reduced by 4%. Nevertheless, the improvements were almost negligible for combinations 1–4, which reduced the bias by 1.5% and the accuracy by 0.5%. Apart from the previous analysis, the positioning errors obtained on each date were compared with the parameters characterising the waves, namely Hs, Tp, run-up, and wave product (Figure 8), as well as the beach slope, showing no significant correlations between those factors and the magnitude of the SDWLs errors.

4. Discussion

Achieving high accuracy and robustness in the shoreline definition on different coastal types constitutes a necessary step before adopting this remote approach for beach monitoring purposes. The evaluation of the different methods and parameters offered by extraction tools and the definition of guidelines for their use is a prerequisite for the widespread application in coastal monitoring systems. The present work evaluates the influence that the extraction parameters and the oceanographic conditions have on the errors of the extracted SDWLs (and, therefore, the SDSs) on a mesotidal and dissipative beach.

4.1. Extraction Parameters and Coastal Conditions Affect SDWL Accuracy

Although the diverse combinations of parameters lead to errors of variable magnitude over the analysed dates, combinations one to four seem to offer more robust and neutral responses under different oceanographic and morphological conditions. These four combinations have in common the employment of the 3 × 3 kernel size and the erosion morphological filter. The 5 × 5 kernel increases the likelihood of finding the real WL even if the initial APS was positioned far from it. However, the higher probability of attaining an acceptable identification of the real boundary comes at the expense of defining it with a lower accuracy, as demonstrated by Sánchez-García et al. [11]. Therefore, the employment of the 3 × 3 kernel allows higher accuracy in the final subpixel SDWL, but it requires a correct definition of the APS, otherwise leading to very gross errors. In La Victoria Beach, the usage of the 3 × 3 kernel in combination with the most favourable combinations of extraction parameters did not lead to gross errors, probably because neither the shoreline nor the instantaneous waterlines experienced great positioning differences along the studied time frame. The definition of an APS with an acceptable level of error relies on the correct selection of the extraction parameters previously employed in the extraction workflow, i.e., index, thresholding method and morphological filter.

In La Victoria Beach, the application of the morphological filter of erosion on the water mask for the definition of the APS consistently leads to SDWLs with higher accuracy than when applying the dilation (see Tables 3 and 4, and Figure 6). Thus, combination one (AWEInsh index, with thresholding = 0, erosion filter and 3 × 3 kernel size) offers the best performance, with seaward bias = 2.70 m, SD = 2.28 m, and overall accuracy = 5.96 m RMSE. The application of the dilation filter leads in all cases to a substantially higher bias, which translates into errors above 10 m RMSE. The reason why the erosion outperforms the dilation filter lies in the type of coast. La Victoria is a tidal, low-gradient and exposed beach

that mainly shows a dissipative behaviour [41]. This translates into situations in which the emerged beach presents patches of water and saturated sand [35]. The definition of the WL in this type of environment is extremely challenging. During low tide conditions, those beaches may present large wet and saturated patches and complex forms [29], sometimes leading to wet/dry boundaries which are optically similar to a waterline interface [42]. Extraction algorithms may experience difficulties in distinguishing the land and the water classes, often creating important errors and biases (e.g., [18,26,30]).

Vos et al. [13] benchmarked the extraction tools CASSIE [12], CoastSat [10], HighTide-SDS [43], ShorelineMonitor [44], and SHOREX [11]. Results evidenced a consistent landward bias on the beaches of Torrey Pines, USA (MSTR 2.3 m, tan β = 0.04) and, more markedly, on the energetic Truc Vert, SW France (MSTR 3.2 m, tan β = 0.04), probably due to the challenges posed by the complex morphologies [29]. In line with that, the assessment of CoastSat by Konstantinou et al. [30] presented a consistent seaward bias of 6.5 m in the reflective beach of Slapton, UK (tan β = 0.13) versus a 4.2 m landward bias in the dissipative site Perranporth, UK (tan β = 0.016) although with far lower accuracy. These findings align with the preliminary assessment of SAET [18], indicating that the lowest errors (and usually small seaward biases) appear in low-energy microtidal sites and less energetic beaches. This occurred contrary to the tidal coasts with gentle slopes and dissipative behaviour (e.g., the Dutch coast) as well as highly energetic beaches (Mira, N Portugal) in which the landward bias commonly appeared, and the application of the erosion filter seemed to enable a better SDWL accuracy. Thus, although an increased level of errors seems to be expected in dissipative beaches as well as in those presenting gentler slopes as they are more prone to show complex intertidal morphologies and water-saturated sands, the employment of different combinations of extraction parameters may help to deal with this challenging morphological reality and minimise the SDWLs errors.

The application of the erosion filter over the water mask instead of the dilation leads to an APS shifted one pixel seaward. This compensates for the lack of a clear water/land boundary that usually tends to displace the SDWL position landward and minimises the bias of the final SDWL. Although C4 (3 $\times$ 3, Erosion, MNDWI, Otsu) leads to a lower bias landward (0.82 m), the higher SD translates into a worse level of accuracy (7.22 m RMSE). When the AWEInsh index is capable of correctly assigning positive (negative) values for the land (water), the thresholding employing a constant value of 0 seems the most simple and convenient solution to achieve a good positioning of the APS. On the contrary, when the water/land distinction is not properly accomplished, the Otsu method appears as a useful alternative. When combined with the MNDWI index, Otsu offers the best results. This method computes the optimal threshold value by analysing the distribution of pixel intensities in the image [21]. This adaptability makes it more suitable for images with varying lighting conditions and content, which probably did not constitute a significant advantage in the present assessment, considering the small size of the site and the lack of cloudy images.

Even though C1 and C4 reach a comparable level of error, it seems reasonable to recommend the use of C1 in this beach type. Among the combinations employing the dilation filter, the best performance is provided when the dilation filter is combined with the AWEInsh index and the thresholding = 0 (C5), which was proposed by Pardo-Pascual et al. [18] as the best solution in reflective beaches. In contrast, in the dissipative beach of La Victoria, this solution leads to an accuracy of 9.34 m RMSE with a significant landward bias (8.76 m). Both solutions (C1 and C5) are best sustained on the employment of the same index, threshold and kernel size. This implies that the AWEInsh index and the threshold = 0 perform well together when defining the water mask. Subsequently, and depending on the beach type (reflective or dissipative), the morphological filter (erosion or dilation) can be chosen to adapt the extraction tool in order to offer higher waterline (shoreline) accuracies. In turn, C5 could constitute a compromise solution for intermediate beaches or those with changeable behaviour over time.

The performance of the different extraction methods differs according to the diverse potential sources of error (such as foam, tide, swash and the presence of water or humidity on the beach surface). The influence of the tide is more evident in some combinations of parameters. Errors do not appear significantly linked to low tide levels when using C1 and C4, whereas when employing C2, up to 1/3 of the bias and half of the overall accuracy appear inversely related (and potentially caused) by the tide level. Thus, SDWLs obtained with a tide level below 2 m appear consistently biased landward.

The challenges posed by the shoreline definition at tidal environments can be observed on La Victoria Beach when comparing the positioning of SDWLs obtained during low tide conditions. Thus, on 22 January 2018 (Figure 9a, MSL = −1.087 m), the SDWLs extracted from C2 and C3 tend to define the limit of the wet areas instead of the land/water limit, causing a large bias. On the other hand, combinations one and four were not affected by this increase in error. This behaviour can be explained by the flooding of the inner part of the beach on its southern half. The 16 July waterlines (Figure 9b, MSL = −1.207 m) present important accuracy differences among the different combinations of parameters. While the SDWL from C1 shows a very high accuracy, C2 experiences an important bias landward.

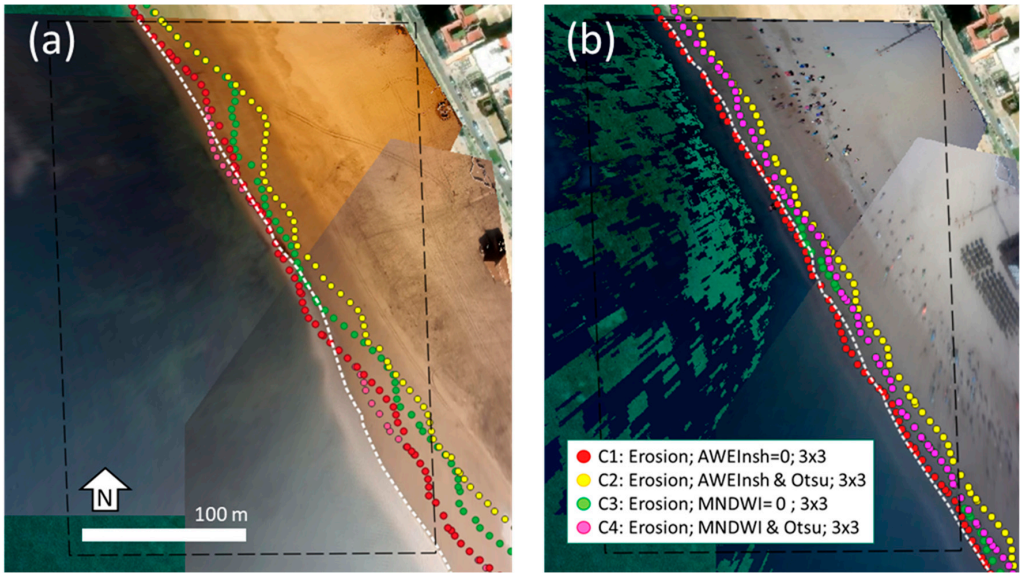

Figure 9. Satellite-derived waterlines on 22 January 2018 (**a**), and 16 July 2018 (**b**) extracted with the combinations 1–4 of extraction parameters together with the VDWL (white dashed line). Timex images are overlapping the orthophotograph PNOA 2019. The study area is delimited by a black dashed line.

The relationship between the tidal level and the errors would not necessarily be linear, and the correlations presented in Table 5 would not be optimal for explaining the phenomenon (in fact, non-linear functions increase the fit R^2 above 0.60). Above a certain tide level, the SDWL errors remain moderate, whereas below that threshold, the waterline definition becomes more challenging, and the reliability of the SDWLs decreases. When discarding low tide dates, the error reduction is only subtle or non-existent for the combinations that already offered the highest accuracies (C1–C4). The different response of each combination to the tide level suggests that the most robust combinations are those with fewer difficulties in distinguishing water and land classes, therefore being less susceptible to associated phenomena such as the presence of wet or saturated areas on the beach surface. While the elimination of images acquired at lower tidal elevations has been proposed as a method for obtaining more accurate shoreline series (e.g., [29]), this strategy was not useful on the dissipative site of Perranporth [30]. The differences would lie in the shape of the lower intertidal section of the profile. La Victoria Beach commonly presents a large diversity of morphologies, such as bars and cusp systems [34] and a rocky shore platform

that extends discontinuously across the area, varying in width and depth and exposed in spring low tides [31,32]. Discarding images during low tide could reduce the errors associated with those complex forms only when the extraction is carried out employing the less precise combinations of parameters. On the contrary, when employing the more robust combinations of parameters, the APS would be properly located, and the discarding of these images would not lead to a significant reduction in errors.

Wave characteristics, in combination with beach morphology, seem to constitute a source of error for certain combinations of parameters. The presence of waves breaking very close to the shore and the appearance of foam (white-water) are related to a seaward bias of C1 and C4 (Figure 10). Thus, the 27 April C1 and C4 describe a similar positioning influenced by the presence of foam, while C2 and C3 appear better describing the WL. This biased positioning associated with C1 led to a lower precision in the SDWL delineation. Similarly, on 22 May, C1 led to large errors despite the high tide level, probably caused by the breaking waves near the beach and the generation of wave foam. This source of error has been previously pointed out by different studies (e.g., [22,45]). Apart from that, punctual seaward shifts, when using certain combinations, could be linked to the reflectance from the seafloor [45]. Contrary to the tide level, neither the parameters describing the instantaneous wave conditions (Hs, Tp) nor those derived from them (such as the wave factor and the run-up) could be numerically related to SDWL errors. Similarly, we cannot conclude that any of the tested combinations are more robust or susceptible to errors according to the wave conditions or the presence of foam.

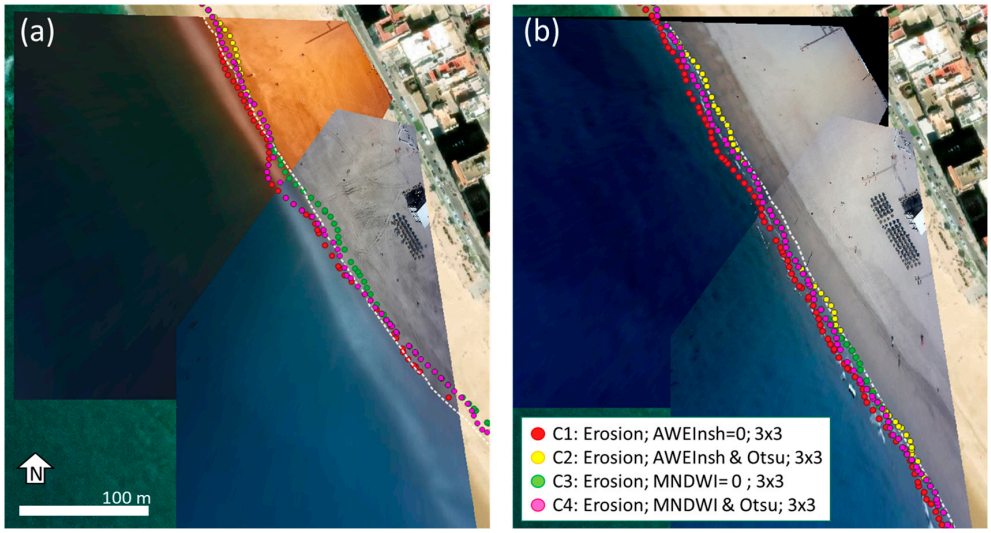

Figure 10. Satellite-derived waterlines extracted with the combinations 1–4 of extraction parameters together with the VDWL (white dashed line) on different dates: (**a**) 27 April 2018, Timex image. Note the high coincidence and overlapping of the points composing the SDWs when using C2 and C3. (**b**) 22 May 2018, Snap image. Background: orthophotograph PNOA 2019.

Certain pairs of SDWLs obtained by e.g., the combinations C1 and C4, and C2 and C3, respectively, show remarkable resemblance. These similarities appear as, in certain cases, those pairs of combinations may propose the same (or very similar) APS. Subsequently, when applying the same sub-pixel algorithm and kernel of analysis, the points composing the resulting SDWLs may be coincident. This behaviour is counterintuitive as they represent different indices (AWEInsh and MNDWI) and thresholding methods (threshold = 0 and Otsu). Errors seem to be partly associated with the landward displacements of the SDWLs extracted when using C2 and C3, probably due to the presence of wet stretches on the emerged beach. In contrast, C1 and C4 combinations are generally more robust, and the errors appear motivated by phenomena affecting all the combinations, such as the presence of foam.

4.2. The Uncertainty in the Waterline Definition in Dissipative Coastal Environments

This assessment relies on the comparison of SDWLs against VDWLs that define the water's edge boundary. This work has employed the Timex images as their interpretation is considered to be more robust. While the Snap images provide an accurate instantaneous representation of the morphological state of the shore, almost synchronous with the satellite imagery, the Timex images consider the dynamism taking place (for 10 min) just before, also allowing us to appreciate the breaking waves with the presence of foam. Nevertheless, the high dynamism of the coastline, together with a combination of tidal and wave-driven processes, may create fuzzy interfaces that challenge the definition of the waterline position. This aspect is particularly important in the case of La Victoria Beach (Cádiz) since it is a meso-tidal beach with large variations in water levels. On certain dates, especially during low tides, the definition of the waterline is challenging even for experienced photo-interpreters as there is not an evident boundary defining the WL. Taking this into account and prior to the use of VDWLs as ground-truth data, a validation of the manual photo-interpretation processes was performed (see Figure 4). One date (21 February) was discarded from the analysis due to the important differences in the waterline definition carried out by both photo-interpreters, particularly over the northern part of the study area (Figure 11). On that day, significant discrepancies appeared among both VDWLs (defined by P1 and P2) when using the same type of image (Timex and Snap), but also when the same user employed different types of images. This was largely motivated by the presence of water-covered areas produced by the tidal ebb, also possibly influenced by the high range of the spring tides that occurred a few days earlier (17–19 February). This is an example of another source of uncertainty in the analysis that hinders photo interpretations in mesotidal environments and with the presence of mesoforms.

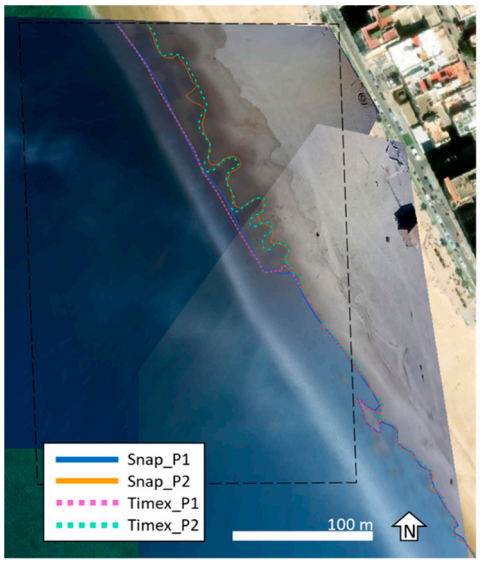

Figure 11. VDWLs defined by two photo-interpreters employing the Snap (solid lines) and the Timex (dashed lines) images on 21 February 2018 during conditions of low tide (SL = 0.95 m), low waves (Hs = 0.6 m) and long period (Tp = 9.89 s) after a large swell episode. Timex image overlapping the PNOA 2019 orthophotograph in the background. The study area is delimited by a black dashed line.

4.3. From SDWL to SDS

The position defined by the SDWLs is a consequence of the water level at the moment of the acquisition of the satellite image. In beaches such as La Victoria, tide and wave conditions lead to very changeable water levels. Referring all the SDWLs to the same datum by removing the effect of the varying water level on the waterline positions leads to their transformation in SDSs, enabling their comparison over time [25,26].

In tidal environments, there is an agreement regarding the suitability of applying a horizontal correction according to the instantaneous tidal conditions. On the contrary, the number of analysis including the application of wave set-up (e.g., [13,46]) and run-up corrections (e.g., [29]) is limited, and the issue is still a matter of debate. Depending on the specific site, some authors suggest that the waterline could represent the upper part or one portion of the swash [28], while others consider that depending on the beach type, the waterline would be closer to the downrush limit or still water level [30]. Anyway, the run-up correction makes sense if accurate slope and wave data are available and if there is certainty about which morphological reality is being represented.

4.4. Future Research

Further assessments employing a larger number of SDWLs and simultaneous VDWLs, as well as a variety of coastal sites, are required to progress in this field. In complex environments such as La Victoria Beach, one year of data (with 18 images) may not be enough to fully capture the variability of conditions, which might not be seasonal but interannual [35]. The availability of more data (i.e., long SDWLs series obtained along a broader tidal range) could allow us to explore more deeply the influence that parameters and coastal conditions have on the shoreline definition. A larger dataset could enable us to accurately define the elevation threshold below which the reliability of the SDWL starts to decrease in this beach, as well as to establish statistical relationships between the punctual oceanographic and morphological conditions and the SDWLs' errors.

Carrying out shoreline accuracy assessments on new beaches and coastal types is a required step to validate and subsequently exploit the potential of shoreline extraction tools around the globe. The extraction processes still present plenty of challenges in certain environments, such as macrotidal beaches. In this regard, the combination of different extraction parameters, as presented in this paper, may have a key role in the definition and integration within the aforementioned tools of new proxies for those coastal types. Particularly, the possibility of using proxies that can be mapped automatically (such as the wet/dry line) constitutes an interesting research issue [13]. The improvement of methods for water level corrections and removal of flawed images also constitutes an interesting challenge in high-energy tidal coasts [42]. Furthermore, although the broad diversity of parameters included in SAET has been tested, new indices and classification alternatives such as k-means or machine learning may help to provide more accurate results [15,23].

5. Conclusions

This assessment constitutes a further step in the validation of SAET to provide a robust and accurate definition of the SDSs, therefore constituting a useful tool for coastal monitoring. The assessment of the shoreline accuracy carried out in the mesotidal and dissipative beach of La Victoria allows the understanding of the influence of the particular morphological and oceanographic conditions in the shoreline definition, as well as proposing solutions to deal with them by exploiting the adaptative capabilities of extraction tools as SAET.

Dissipative beaches are more prone to present complex intertidal morphologies and water-saturated sands that pose a challenge when identifying the waterline position. Nevertheless, the employment of different combinations of extraction parameters may help to compensate for this challenging morphological reality and minimise the SDWL errors. Specific conditions of waves, tide level and range, beach slope and presence of mesoforms seem to contribute to reducing the accuracy of results. Nevertheless, apart from the clear effect of the tidal level when using certain combinations of extraction parameters, no solid numerical relationship could be found between the positioning errors on each date and the associated morphological and oceanographic conditions, maybe because of the limited number of dates that have been analysed. The expansion of the dataset could lead to a deeper exploration of these relationships.

Anyway, certain combinations of parameters seem not to be greatly affected by the aforementioned factors and offer robust results regardless of the changeable conditions. In this dissipative site, the combination of the AWEInsh index with thresholding = 0, the erosion morphological filter and 3 × 3 kernel size leads to the highest accuracy overall. Our results suggest that, when defining the approximate shoreline at pixel level from the water mask, the application of the morphological filter of erosion is a useful and novel strategy to overcome the landward bias that commonly occurs in dissipative beaches. This occurs contrary to the significantly larger landward bias obtained when using the dilation filter, which seems to be more convenient for the shoreline definition on beaches with a clearer water/land interface and reflective behaviour.

Together with previous studies, this assessment underlines the lack of solutions for defining the shoreline that can be applied automatically at a global level. Thus, the application of extraction parameters on dissipative beaches that gave good accuracy on reflective coasts leads to significantly biased SDWLs. This idea stresses the need to adapt and validate the shoreline extraction methodologies to the different types of coastlines as an essential prior step for the characterisation and interpretation of geomorphological changes on the different coasts of the planet.

Author Contributions: Conceptualization, C.C.-R., J.A.-C., J.B., B.C., L.D.R., J.M., J.P.-V. and J.E.P.-P.; Software, C.C.-R., J.A.-C., J.P.-V. and J.E.P.-P.; Data curation, C.C.-R., J.A.-C., J.P.-V. and J.E.P.-P.; Writing—original draft, C.C.-R.; Writing—review & editing, C.C.-R., J.A.-C., J.B., B.C., L.D.R., J.M., J.P.-V. and J.E.P.-P.; Visualization, C.C.-R. and J.M.; Project administration, C.C.-R., L.D.R., J.M. and J.E.P.-P.; Funding acquisition, C.C.-R., L.D.R., J.M. and J.E.P.-P. All authors have read and agreed to the published version of the manuscript.

Funding: This research was funded by the projects MONOBESAT (PID2019-111435RB-I00) by the Spanish Ministry of Science, Innovation and Universities; CRISIS (Coastal Risk Evaluation Under Climate Change Scenarios), by the Spanish Ministry of Science and Innovation (PID2019-109143RB-I00); the grants PAID-06-22 (CCR) by the Vicerrectorado de Investigación de la Universitat Politècnica de València (UPV), and PR-2023-032 (JM) by Universidad de Cádiz (UCA); CCR and JM were funded by MS contracts within the Re-qualification programme by the Spanish Ministry of Universities also financed by the EU—NextGenerationEU; BC by Agence Nationale de la Recherche (ANR) grant number ANR-21-CE01-0015.

Data Availability Statement: The data presented in this study are available in article.

Acknowledgments: The authors acknowledge Puertos del Estado and IEO for the oceanographic data, IGN for the orthophotography, and ESA for the S2 imagery.

Conflicts of Interest: The authors declare no conflict of interest.

References

1. Boak, E.H.; Turner, I.L. Shoreline Definition and Detection: A Review. *J. Coast. Res.* **2005**, *214*, 688–703. [CrossRef]
2. Castelle, B.; Ritz, A.; Marieu, V.; Lerma, A.N.; Vandenhove, M. Primary drivers of multidecadal spatial and temporal patterns of shoreline change derived from optical satellite imagery. *Geomorphology* **2022**, *413*, 108360. [CrossRef]
3. Vos, K.; Harley, M.D.; Turner, I.L.; Splinter, K.D. Pacific shoreline erosion and accretion patterns controlled by El Niño/Southern Oscillation. *Nat. Geosci.* **2023**, *16*, 140–146. [CrossRef]
4. Calkoen, F.; Luijendijk, A.; Rivero, C.R.; Kras, E.; Baart, F. Traditional vs. Machine-Learning Methods for Forecasting Sandy Shoreline Evolution Using Historic Satellite-Derived Shorelines. *Remote Sens.* **2021**, *13*, 934. [CrossRef]
5. Cabezas-Rabadán, C.; Pardo-Pascual, J.; Almonacid-Caballer, J.; Rodilla, M. Detecting problematic beach widths for the recreational function along the Gulf of Valencia (Spain) from Landsat 8 subpixel shorelines. *Appl. Geogr.* **2019**, *110*, 102047. [CrossRef]
6. Cabezas-Rabadán, C.; Pardo-Pascual, J.E.; Palomar-Vázquez, J.; Fernández-Sarría, A. Characterizing beach changes using high-frequency Sentinel-2 derived shorelines on the Valencian coast (Spanish Mediterranean). *Sci. Total Environ.* **2019**, *691*, 216–231. [CrossRef]
7. Molina, R.; Anfuso, G.; Manno, G.; Gracia Prieto, F.J. The Mediterranean Coast of Andalusia (Spain): Medium-Term Evolution and Impacts of Coastal Structures. *Sustainability* **2019**, *11*, 3539. [CrossRef]
8. Laksono, F.A.T.; Borzi, L.; Distefano, S.; Czirok, L.; Halmai, Á.; Di Stefano, A.; Kovács, J. Shoreline change dynamics along the Augusta coast, eastern Sicily, South Italy. *Earth Surf. Process. Landf.* **2023**, *48*, 2630–2641. [CrossRef]

9. Vitousek, S.; Buscombe, D.; Vos, K.; Barnard, P.L.; Ritchie, A.C.; Warrick, J.A. The future of coastal monitoring through satellite remote sensing. *Camb. Prism. Coast. Futures* **2023**, *1*, e10. [CrossRef]
10. Vos, K.; Splinter, K.D.; Harley, M.D.; Simmons, J.A.; Turner, I.L. CoastSat: A Google Earth Engine-enabled Python toolkit to extract shorelines from publicly available satellite imagery. *Environ. Model. Softw.* **2019**, *122*, 104528. [CrossRef]
11. Sánchez-García, E.; Palomar-Vázquez, J.; Pardo-Pascual, J.; Almonacid-Caballer, J.; Cabezas-Rabadán, C.; Gómez-Pujol, L. An efficient protocol for accurate and massive shoreline definition from mid-resolution satellite imagery. *Coast. Eng.* **2020**, *160*, 103732. [CrossRef]
12. Almeida, L.P.; de Oliveira, I.E.; Lyra, R.; Dazzi, R.L.S.; Martins, V.G.; da Fontoura Klein, A.H. Coastal analyst sys-tem from space imagery engine (CASSIE): Shoreline management module. *Environ. Model. Softw.* **2021**, *140*, 105033. [CrossRef]
13. Vos, K.; Splinter, K.D.; Palomar-Vázquez, J.; Pardo-Pascual, J.E.; Almonacid-Caballer, J.; Cabezas-Rabadán, C.; Kras, E.C.; Luijendijk, A.P.; Calkoen, F.; Almeida, L.P.; et al. Benchmarking satellite-derived shoreline mapping algorithms. *Commun. Earth Environ.* **2023**, *4*, 345. [CrossRef]
14. Pardo-Pascual, J.E.; Almonacid-Caballer, J.; Ruiz, L.A.; Palomar-Vázquez, J. Automatic extraction of shorelines from Landsat TM and ETM+ multi-temporal images with subpixel precision. *Remote Sens. Environ.* **2012**, *123*, 1–11. [CrossRef]
15. Palomar-Vázquez, J.; Pardo-Pascual, J.E.; Almonacid-Caballer, J.; Cabezas-Rabadán, C. Shoreline Analysis and Extraction Tool (SAET): A New Tool for the Automatic Extraction of Satellite-Derived Shorelines with Subpixel Accuracy. *Remote Sens.* **2023**, *15*, 3198. [CrossRef]
16. Xu, H. Modification of normalised difference water index (NDWI) to enhance open water features in remotely sensed imagery. *Int. J. Remote Sens.* **2006**, *27*, 3025–3033. [CrossRef]
17. Feyisa, G.L.; Meilby, H.; Fensholt, R.; Proud, S.R. Automated Water Extraction Index: A new technique for surface water mapping using Landsat imagery. *Remote Sens. Environ.* **2014**, *140*, 23–35. [CrossRef]
18. Pardo-Pascual, J.E.; Almonacid-Caballer, J.; Cabezas-Rabadán, C.; Fernández-Sarría, A.; Armaroli, C.; Ciavola, P.; Montes, J.; Souto-Ceccon, P.E.; Palomar-Vázquez, J. Assessment of satellite-derived shorelines automatically extracted from Sentinel-2 imagery using SAET. *Coast. Eng.* **2024**, *188*, 104426. [CrossRef]
19. Palomar-Vázquez, J.; Cabezas-Rabadán, C.; Castañeda, C.; Gracia, F.J.; Fernández-Sarría, A.; Priego-De-Los-Santos, E.; Pons-Crespo, R.; Pardo-Pascual, J.E. Inferring volumetric changes at a shallow lake from subpixel satellite-derived shorelines. *Appl. Geogr.* **2022**, *149*, 102792. [CrossRef]
20. Bishop-Taylor, R.; Sagar, S.; Lymburner, L.; Alam, I.; Sixsmith, J. Sub-Pixel Waterline Extraction: Characterising Accuracy and Sensitivity to Indices and Spectra. *Remote Sens.* **2019**, *11*, 2984. [CrossRef]
21. Otsu, N. A threshold selection method from gray-level histograms. *IEEE Trans. Syst. Man Cybern.* **1979**, *9*, 62–66. [CrossRef]
22. Hagenaars, G.; de Vries, S.; Luijendijk, A.P.; de Boer, W.P.; Reniers, A.J. On the accuracy of automated shoreline detection derived from satellite imagery: A case study of the sand motor mega-scale nourishment. *Coast. Eng.* **2018**, *133*, 113–125. [CrossRef]
23. McAllister, E.; Payo, A.; Novellino, A.; Dolphin, T.; Medina-Lopez, E. Multispectral satellite imagery and machine learning for the extraction of shoreline indicators. *Coast. Eng.* **2022**, *174*, 104102. [CrossRef]
24. Haralick, R.M.; Sternberg, S.R.; Zhuang, X. Image analysis using mathematical morphology. *IEEE Trans. Pattern Anal. Mach. Intell.* **1987**, *PAMI-9*, 532–550. [CrossRef]
25. Vitousek, S.; Vos, K.; Splinter, K.D.; Erikson, L.; Barnard, P.L. A model integrating satellite-derived shoreline observations for predicting fine-scale shoreline response to waves and sea-level rise across large coastal regions. *J. Geophys. Res. Earth Surf.* **2023**, *128*, e2022JF006936. [CrossRef]
26. Vos, K.; Harley, M.D.; Splinter, K.D.; Simmons, J.A.; Turner, I.L. Sub-annual to multi-decadal shoreline variability from publicly available satellite imagery. *Coast. Eng.* **2019**, *150*, 160–174. [CrossRef]
27. Almonacid-Caballer, J.; Pardo-Pascual, J.E.; Ruiz, L.A. Evaluating Fourier Cross-Correlation Sub-Pixel Registration in Landsat Images. *Remote Sens.* **2017**, *9*, 1051. [CrossRef]
28. Cabezas-Rabadán, C.; Pardo-Pascual, J.E.; Palomar-Vázquez, J.; Ferreira, Ó.; Costas, S. Satellite Derived Shorelines at an Exposed Meso-tidal Beach. *J. Coast. Res.* **2020**, *95*, 1027–1031. [CrossRef]
29. Castelle, B.; Masselink, G.; Scott, T.; Stokes, C.; Konstantinou, A.; Marieu, V.; Bujan, S. Satellite-derived shoreline detection at a high-energy meso-macrotidal beach. *Geomorphology* **2021**, *383*, 107707. [CrossRef]
30. Konstantinou, A.; Scott, T.; Masselink, G.; Stokes, K.; Conley, D.; Castelle, B. Satellite-based shoreline detection along high-energy macrotidal coasts and influence of beach state. *Mar. Geol.* **2023**, *462*, 107082. [CrossRef]
31. Gracia, F.; Rodriguezvidal, J.; Cáceres, L.; Belluomini, G.; Benavente, J.; Alonso, C. Diapiric uplift of an MIS 3 marine deposit in SW Spain: Implications for Late Pleistocene sea level reconstruction and palaeogeography of the Strait of Gibraltar. *Quat. Sci. Rev.* **2008**, *27*, 2219–2231. [CrossRef]
32. Muñoz-Perez, J.J.; Medina, R. Comparison of long-, medium-and short-term variations of beach profiles with and without submerged geological control. *Coast. Eng.* **2010**, *57*, 241–251. [CrossRef]
33. Puig, M. Análisis de las Variables que Controlan la Evolución de la Costa a Corto-Medio Plazo. Aplicación a la Bahía de Cádiz. Ph.D. Thesis, University of Cádiz, Cádiz, Spain, 2016.
34. Montes, J.; Simarro, G.; Benavente, J.; Plomaritis, T.A.; Del Río, L. Morphodynamics Assessment by Means of Mesoforms and Video-Monitoring in a Dissipative Beach. *Geosciences* **2018**, *8*, 448. [CrossRef]

35. Montes, J.; del Río, L.; Plomaritis, T.A.; Benavente, J.; Puig, M.; Simarro, G. Video-Monitoring Tools for Assessing Beach Morphodynamics in Tidal Beaches. *Remote Sens.* **2023**, *15*, 2650. [CrossRef]
36. Vousdoukas, M.I.; Ferreira, P.M.; Almeida, L.P.; Dodet, G.; Andriolo, U.; Psaros, F.; Taborda, R.; Silva, A.N.; Ruano, A.E.; Ferreira, Ó. Performance of intertidal topography video monitoring of a meso-tidal reflective beach in South Portugal. *Ocean Dyn.* **2011**, *61*, 1521–1540. [CrossRef]
37. Sánchez-García, E.; Balaguer-Beser, A.; Pardo-Pascual, J.E. C-Pro: A coastal projector monitoring system using terrestrial photogrammetry with a geometric horizon constraint. *ISPRS J. Photogramm. Remote Sens.* **2017**, *128*, 255–273. [CrossRef]
38. Simarro, G.; Ribas, F.; Álvarez, A.; Guillén, J.; Chic, Ò.; Orfila, A. ULISES: An open-source code for extrinsic calibrations and planview generations in coastal video monitoring systems. *J. Coast. Res.* **2017**, *33*, 1217–1227. [CrossRef]
39. Graham, R.; Hell, P. On the History of the Minimum Spanning Tree Problem. *IEEE Ann. Hist. Comput.* **1985**, *7*, 43–57. [CrossRef]
40. Stockdon, H.F.; Holman, R.A.; Howd, P.A.; Sallenger, A.H., Jr. Empirical Parameterization of Setup, Swash, and Runup. *Coast. Eng.* **2006**, *53*, 573–588. Available online: https://www.sciencedirect.com/science/article/pii/S0378383906000044?via=ihub (accessed on 10 January 2023). [CrossRef]
41. Benavente, J.; Plomaritis, T.A.; del Río, L.; Puig, M.; Valenzuela, C.; Minuzzi, B. Differential short- and medium-term behavior of two sections of an urban beach. *J. Coast. Res.* **2014**, *70*, 621–626. [CrossRef]
42. Graffin, M.; Taherkhani, M.; Leung, M.; Vitousek, S.F.; Kaminsky, G.; Ruggiero, P. Monitoring interdecadal coastal change along dissipative beaches via satellite imagery at regional scale. *Camb. Prism. Coast. Futures* **2023**, *1*, e42. [CrossRef]
43. Mao, Y.; Harris, D.L.; Xie, Z.; Phinn, S. Efficient measurement of large-scale decadal shoreline change with increased accuracy in tide-dominated coastal environments with Google Earth Engine. *ISPRS J. Photogramm. Remote Sens.* **2021**, *181*, 385–399. [CrossRef]
44. Luijendijk, A.; Hagenaars, G.; Ranasinghe, R.; Baart, F.; Donchyts, G.; Aarninkhof, S. The State of the World's Beaches. *Sci. Rep.* **2018**, *8*, 6641, Correction in **2018**, *8*, 11381. [CrossRef]
45. Pardo-Pascual, J.E.; Sánchez-García, E.; Almonacid-Caballer, J.; Palomar-Vázquez, J.M.; Priego de los Santos, E.; Fernández-Sarría, A.; Balaguer-Beser, Á. Assessing the Accuracy of Automatically Extracted Shorelines on Microtidal Beaches from Landsat 7, Landsat 8 and Sentinel-2 Imagery. *Remote Sens.* **2018**, *10*, 326. [CrossRef]
46. Cabezas-Rabadán, C.; Pardo-Pascual, J.E.; Palomar-Vázquez, J.; Roch-Talens, A.; Guillén, J. Satellite observations of storm erosion and recovery of the Ebro Delta coastline, NE Spain. *Coast. Eng.* **2024**, *188*, 104451. [CrossRef]